Noname manuscript No.
(will be inserted by the editor)

Aerodynamic properties of an archery arrow

Takeshi Miyazaki · Keita Mukaiyama · Yuta Komori · Kyouhei Okawa · Satoshi Taguchi · Hiroki Sugiura

Received: date / Accepted: date

Abstract Two support-interference-free measurements of aerodynamic forces exerted on an archery arrow (A/C/E; Easton) are described. The first measurement is conducted in a wind tunnel with JAXA's 60 cm Magnetic Suspension and Balance System (MSBS), in which an arrow is suspended and balanced by magnetic force against gravity. The maximum wind velocity is 45 m/sec, which is less than a typical velocity of an arrow (about 60 m/sec) shot by an archer. The boundary layer of the arrow remains laminar in the measured Re number range ($4.0 \times 10^3 < Re < 1.5 \times 10^4$), and the drag coefficient is about 1.5 for $Re > 1.0 \times 10^4$. The second measurement is performed by a free flight experiment. Using two high-speed video cameras, we record the trajectory of an archery arrow and analyze its velocity decay rate, from which the drag coefficient is determined. In order to investigate Re number dependence of the drag coefficient in a wider range ($9.0 \times 10^3 < Re < 2.4 \times 10^4$), we have developed an arrow-shooting system using compressed air as a power source, which launches the A/C/E arrow at an arbitrary velocity up to 75 m/sec. We attach two points (piles) of different type (streamlined and bullet) to the arrow-nose. The boundary layer is laminar for both points for Re less than about 1.2×10^4. It becomes turbulent for Re larger than 1.2×10^4 and the drag coefficient increases to about 2.6, when the bullet point is attached. In the same Re range, two values of drag coefficient are found for the streamlined point, of which the lower value is about 1.6 (laminar boundary layer) and the larger value is

T. Miyazaki, K. Mukaiyama, Y. Komori, K. Okawa, S. Taguchi
Department of Mechanical Engineering and Intelligent Systems,
Graduate School of Informatics and Engineering,
University of Electro-Communications,
1-5-1 Chofugaoka, Chofu, Tokyo 182-8585, Japan
E-mail: miyazaki@mce.uec.ac.jp, taguchi@mce.uec.ac.jp

H. Sugiura
JAXA, 7-44-1 Jindaiji-higashimachi, Chofu, Tokyo 182-8522, Japan
E-mail: sugiura.hiroki@jaxa.jp

about 2.6 (turbulent boundary layer), confirming that the point-shape has a crucial influence on the laminar to turbulent transition of the boundary layer.

Keywords Archery arrow · Drag coefficient · Boundary layer transition

1 Introduction

Bows and arrows have long history. They were used in hunting and warfare until the development of gunpowder weapons. In the modern world, they became popular as sports equipment and have been highly refined and improved by modern technologies. As a matter of fact, the winner scores in archery tournaments are soaring higher and higher. There exist a number of investigations on the arrow launching mechanism from the bow, called the internal ballistics [2,13]. They successfully provide a physical interpretation of the archer's paradox, and suggest improvements of the efficiency of the bow and arrow system. In contrast, only a few scientific studies are known on the aerodynamics of an arrow, i.e., the external ballistics. Denny computed flight arrow trajectories in his book [3], where the aerodynamic properties, such as the drag and lift coefficients, were estimated from arrow geometry (e.g., size, shape). Although he obtained reasonable estimates, they were not derived from any reliable experimental measurements. This lack of concrete experimental data is mainly because the motion of an arrow in flight is highly complicated. It oscillates along its length as well as spins around its axis of revolution. It is quite difficult and almost impossible to reproduce these complicated motions in wind tunnel experiments. Even if we ignore the oscillatory motion and consider an arrow as a thin rigid body, any kind of mechanical supporting system used in usual wind tunnel tests, disturbs the flow field seriously and makes the measurement of aerodynamic forces acting on the arrow inaccurate. Foley *et al.* [4] conducted a wind tunnel experiment and estimated the drag to weight ratio of a medieval longbow arrow and several medieval crossbow bolts. Although the details of their wind tunnel tests were not described, they commented that the size of measured projectiles approached the sensitivity limits of their measuring apparatus.

Recently, two methods realizing *support-interference-free measurements* were proposed by our group [11]. First, the aerodynamic forces can be measured accurately in a wind tunnel equipped with JAXA's 60 cm Magnetic Suspension and Balance System (MSBS), in which the force supporting an arrow is generated by magnetic fields. Sawada [8] measured the drag and lift coefficients of a Japanese arrow shaft (without feather) by the MSBS wind tunnel tests. A cone-type point was attached to the arrow nose and the boundary layer became turbulent. Mukaiyama *et al.* [7] investigated the aerodynamics of a crossbow bolt (HORTON), and explored the influence of the point-shape on the boundary layer transition. They attached three points of different type (streamlined, bullet and bluff bodied) to the bolt-nose. The boundary layer was laminar for the streamlined point and turbulent for other points, in the

measured Reynolds number (Re) range ($5.3 \times 10^3 < Re < 5.1 \times 10^4$; the diameter of arrow shaft is used as the length scale). The second method is based on the flight experiments. Primitive flight experiments were performed by experimental archaeologists previously [1], but the results were not discussed in detail from a purely aerodynamic view point. Recently, Mukaiyama *et al.* [7] presented more accurate results (relative error within 12 %) on the drag acting on the crossbow bolt from their flight measurements at a 50 m outdoor archery range. They compared the results of flight measurements in the Re range of $1.4 \times 10^4 < Re < 3.5 \times 10^4$ with those of the MSBS wind tunnel tests to find consistency between them, confirming the ability of both measurements to provide quantitatively reliable data.

In this paper, we investigate the aerodynamics of an archery arrow (A/C/E; Easton) by performing two kinds of support-interference-free measurements. The drag, the lift and the pitching moment exerted on the arrow are measured in the MSBS wind tunnel. The maximum wind velocity is 45 m/sec, and the wind tunnel tests cover the Reynolds number range $4.0 \times 10^3 < Re < 1.5 \times 10^4$. We also perform the flight measurements at the 70 m indoor archery range of Japan Institute of Sports Sciences (JISS). The trajectory and rotation of the arrow in free flight are recorded using two high-speed video cameras 45 m apart. The drag coefficient is determined from the velocity decay rate. An archer can launch his (her) arrow from his (her) bow only at a fixed initial velocity, typically about 60 m/sec. In order to cover a wider velocity-range, an arrow blowing system using compressed air as a power source is newly developed. It can launch the A/C/E arrow at an arbitrary speed up to 75 m/sec at 7 MPa. Two points (bullet and streamlined) are attached to the arrow-nose and their influence on the aerodynamics is investigated in the Re range $9.0 \times 10^3 < Re < 2.4 \times 10^4$.

The paper is organized as follows. We describe the experimental methods in Sec. 2. The results from the two measurements are presented and compared in Sec. 3. In Sec. 4, further results from additional wind tunnel tests are explained in order to discuss the physical significance of our results. Section 5 is devoted to conclusions.

2 Experiments

We describe the details of the two support-interference-free measurements in this section. We measure the aerodynamic properties of an arrow shown in Fig. 1. The arrow consists of a carbon shaft called A/C/E (Easton), the bullet-type point (ACE Screw Point; Easton), and the spin wing vanes (Range-O-Matic Archery). The A/C/E is a barrel-type shaft with the mean external diameter 5.25 mm and the length 625 mm. The total weight including the point and the vanes is 14.3 g. In the flight experiments described later (Sec. 2.2), this arrow was also shot by an expert female archer (36 shots). A streamlined point (brass: hand made) is also attached to the arrow nose instead of the bullet point, in order to investigate its influence on the aerodynamics.

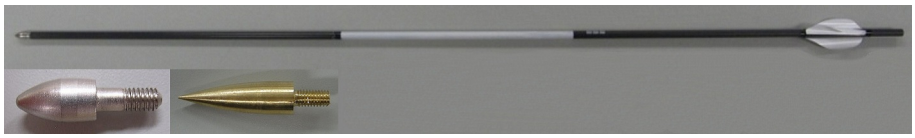

Fig. 1 Archery arrow A/C/E with the bullet and streamlined points

Before going into the details of the measurements, let us summarize the basic fluid dynamical variables. First, the Reynolds number Re is defined as,

$$Re = \frac{\rho DU}{\mu}. \tag{1}$$

Here, D is the mean diameter of the arrow shaft and U denotes the arrow velocity, whereas ρ and μ are the density and the viscosity of the air, respectively. The Reynolds number is the most important non-dimensional parameter to characterize the behavior of viscous fluids..

We also non-dimensionalize the aerodynamic forces, such as the drag F_D, the lift F_L and the pitching moment M:

$$F_D = \frac{\pi}{8} C_D \rho U^2 D^2, \quad F_L = \frac{\pi}{8} C_L \rho U^2 D^2, \quad M = \frac{\pi}{8} C_M \rho U^2 D^2 L. \tag{2}$$

Here, C_D and C_L are the drag and lift coefficients, respectively. C_M denotes the pitching moment coefficient and L is the length of the arrow. These coefficients varies with Re gradually in general, but an abrupt increase of C_D for a streamlined body is observed at a certain Reynolds number known as the critical Reynolds number Re_c, where the transition from the laminar to turbulent boundary layer occurs. It is one of long lasting subjects in fluid mechanics to fully understand the physical mechanism of the boundary layer transition. We will see later that the study of arrow-aerodynamics is not a straightforward application of fluid mechanics, but it casts another puzzle on the subject.

2.1 MSBS wind tunnel experiments

The Magnetic Suspension and Balance System (MSBS) of the JAXA's 60 cm wind tunnel provides an ideal way of supporting a thin arrow for wind tunnel tests, because the force supporting the arrow is generated by magnetic fields which are controlled by 10 coils arranged outside the test section. Figure 2 illustrates the coil arrangement. We insert 10 pieces of cylindrical neodymium magnet of diameter 4 mm and length 30 mm, inside the arrow shaft and the magnetic field is adjusted to balance the gravity by controlling the electric currents flowing the coils. When the wind is flowing, we further adjust the magnetic field to compensate the aerodynamic forces exerted on the arrow, i.e., we control the electric currents so that the arrow remains at a fixed position with an initially specified attitude. The aerodynamic forces, such as the drag, the lift and the pitching moment, are calculated from the values of the required electric currents in order to keep the arrow stationary.

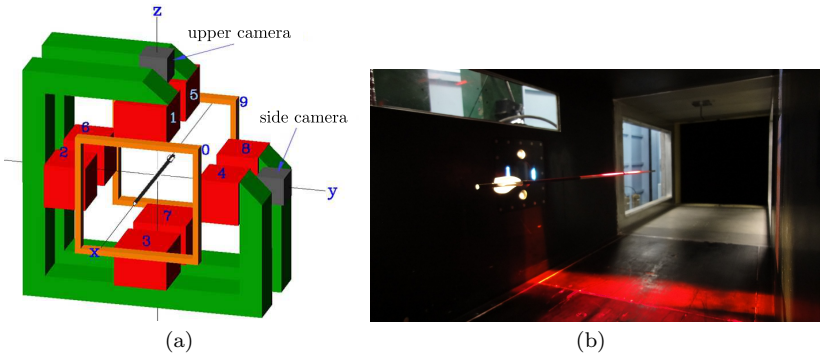

Fig. 2 JAXA's 60 cm magnetic suspension balance system (MSBS): (a) coil arrangement, (b) suspended archery arrow

The accuracy of measurement depends both on the accuracy of the optical sensors of the position and the attitude, and on the control ability, especially the response time (245 Hz) of the feed back circuit, whose details with an error analysis are found in Sawada and Suda [9]. The data are averaged for 1 sec and these mean values are shown in the next section. Generally, the relative error decreases with the wind velocity in wind tunnel tests, because the measured aerodynamic forces increase in proportion to the square of the wind velocity. The maximum wind velocity is 45 m/sec, and the fluctuation level at 30 m/sec is 0.06 %. This maximum velocity is less than the typical launching velocity of the archery arrow 60 m/sec. The measurements are performed for the Re number range $0.4 \times 10^4 < Re < 1.5 \times 10^4$ in the wind tunnel tests. The flight experiments explained in the next subsection are intended to cover a higher velocity (or Re) range.

2.2 Flight experiments

The flight experiments are performed at the indoor archery range of the Japan Institute of Sports Science (JISS). We record the trajectory and the rotation of the arrow in free flight, by two high speed video cameras (Phantom V310: Vision Research Co.), with the spatial resolution of 1280×800 pixels and the temporal resolution 2800 fps. The experimental arrangements are shown in Figure 3. Camera 1 is located 13 m apart from the launching position and Camera 2 is located 45 m further apart from Camera 1. They are placed 3 m side-ward from the line connecting the launching machine and the target center. They record the side views of the flying arrow. We analyze the video images to determine the horizontal and vertical velocity components of the arrow at these two locations, from which we can estimate the drag coefficient C_D assuming that no lift force is acting on the arrow, i.e., the arrow flies ideally with zero angle of attack (see Appendix for the details of analysis).

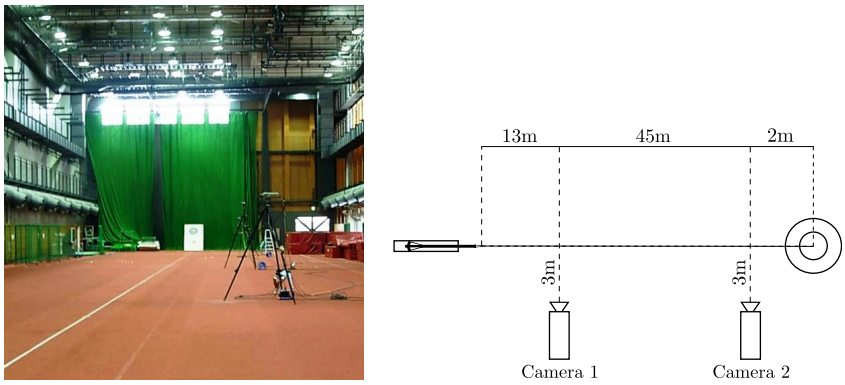

Fig. 3 Apparatus in the flight experiments at the indoor archery range of JISS

The repeatability of arrow launching is the essential point in our flight experiments. This is mainly because the length scale in the video image changes sensitively with the distance between the arrow and the camera. We propose an empirical correction of the length scale in the next section (Sec. 3.3). In addition, the initial velocity should also be repeatable. The accuracy of shots by an elite archer is very high with excellent repeatability. This means that the initial arrow velocity is fixed for each archer, providing a large merit to obtain statistically reliable data at a fixed Re number. However, it can be a demerit in studying wider velocity range. Even if we ask many archers to shoot arrows, the range of their arrow velocities is rather limited around 60 m/sec.

In order to circumvent this difficulty, we have developed a new arrow launching system, It consists of an electric compressor (MAX AK-HL1230E as a power source), a regulator (SMC VCHR30-06G), a sub-tank, an electric valve (SMC VCH41-1D-06G: 5 MPa, KEIHIN SSPD-12GUKD-01: 20 MPa) and a thin nozzle of external diameter 4 mm (Fig. 4). The launching velocity is proportional to the square root of the pressure, and it reaches 62 m/sec at 4.3 MPa, which is the maximum pressure attained by the electric compressor. In order to realize higher velocities, we utilize a special hand pump (FX airguns) used for charging air guns, whose maximum pressure is 25 MPa. We have attained the velocity 75 m/sec at 7 MPa in our experiments. The relative error of the launching velocity is within 0.3 % in the range $0 < U < 62$ m/sec (using the electric compressor), and increases to 0.8 % in the higher velocity range ($62 < U < 75$ m/sec: using the hand pump). Still, the repeatability of our launching system is satisfactory, being comparable with that of an expert female archer (0.6 % at 58 m/sec). The accuracy of shots is also comparable with those of expert archers of the national team.

The video images of about 30 shots are recorded at each Re and the average and the standard deviation of the velocity and the drag coefficient C_D are determined. The number of shots is doubled at Re numbers at which a large data-scattering is observed.

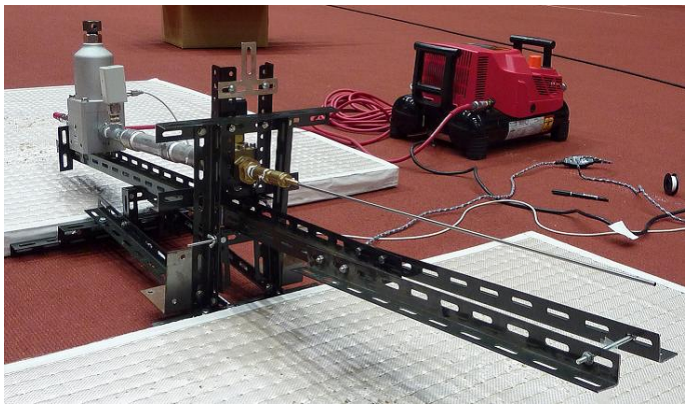

Fig. 4 Arrow launching system using compressed air as a power source

It is worth mentioning that the arrow launched from this launching system only translates and rotates as a rigid body and does not oscillates along its axis. In contrast, the arrow shot from the bow undergoes oscillations along its axis. It is therefore interesting to investigate the influence of this oscillation on the aerodynamic forces. Apart from the oscillation, there is another slight difference between the arrow shot by the bow and that launched by the blowing machine, because the nock is removed when the arrow is launched by the machine. We asked an expert female archer to shoot the same A/C/E arrow (36 shots). As will be seen later, the presence of the nock yields no substantial difference to the drag coefficient, presumably because the boundary layer is thick enough at the rear end of the arrow shaft and the nock is immersed inside the boundary layer.

3 Measurement results

We describe the main results of our measurements in this section, i.e., the Re dependence of the drag coefficient C_D. Unlike for the crossbow bolt [7,11], we will find some differences between the results from the wind tunnel tests and those from the flight experiments. The physical interpretation of these discrepancies is addressed in the next section (Sec. 4).

3.1 Rotation of the arrow

The arrow rotates as it flies due to the aerodynamic effect of the vanes. The rotation rate is proportional to the arrow speed in general, as shown in Fig. 5. Here, the horizontal axis is the arrow speed at Camera 2 (or the wind velocity of the wind tunnel) U_2 (m/sec) and the vertical axis denotes the rotation rate f (rps). The rotation rate is determined by analyzing the image of the high speed video camera. The closed circles show the results from the wind tunnel

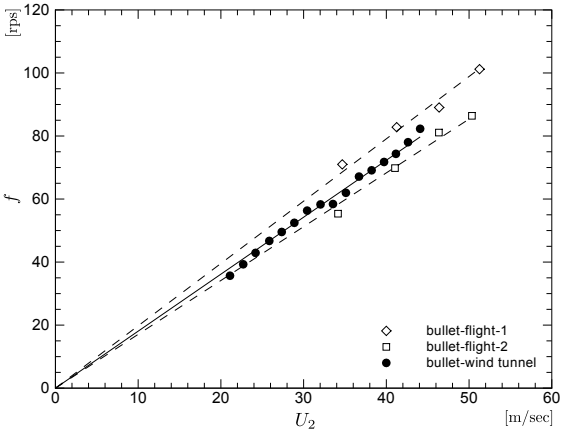

Fig. 5 Arrow rotation rate f as a function of the velocity U_2

measurements and the squares and diamonds show the results from two series of flight experiments. The bullet type point is attached to the arrow nose.

There are some differences between the inclinations of the three lines, because the vanes are refletched whenever they are damaged in the experiments. The rotation rate is non-dimensionalized as a spin parameter $Sp = \pi Df/U_2$, which is sensitive to the situation of the fletched vanes. The values of $Sp = 0.030$ (wind tunnel: solid line) and $Sp = 0.028, 0.033$ (flight: two broken lines) are very small both in the wind tunnel experiment and the flight experiments. We see below that such small differences in Sp have no significant influence on C_D.

3.2 Drag coefficient from the MSBS wind tunnel experiments

Figure 6 illustrates the dependence of C_D on the Reynolds number Re, obtained in the MSBS wind tunnel experiments. The solid line shows the theoretical estimate based on the classical power series solution (the Seban-Bond-Kelly solution [6,10]) for the laminar boundary layer developed on the surface of a circular cylinder. The symbols + and $\diamond$ denote the results for the bare arrow shaft (with no vane) with the bullet and the streamlined points, respectively. No difference can be seen between them and therefore we can conclude that the boundary layer remains laminar in the range $Re < 1.35 \times 10^4$. The small difference about 0.15 from the theoretical value is due to the base drag.

The closed circles and triangles denote the results for the fletched arrow. The former correspond to the bullet point and the latter to the streamlined point. We can see again almost no difference between the two results. Their values are larger than those of bare shafts by the amount of about 0.75, which is due to the friction drag acting on the vanes. Although the fletched arrow rotates as shown in Figure 5, the boundary layer remains laminar in the mea-

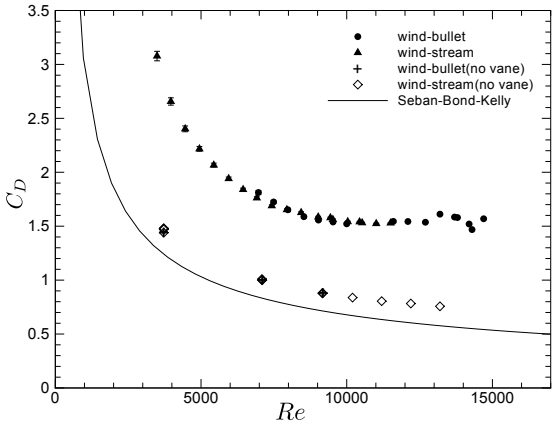

Fig. 6 C_D as a function of Re: MSBS wind tunnel tests

sured Re range, i.e., less than about 1.5×10^4. It is also noted that C_D is almost constant (about 1.5) for $1.0 \times 10^4 < Re < 1.5 \times 10^4$.

3.3 Drag coefficient from the flight experiments

Before presenting the results for the flight experiments, we explain an empirical data-correction procedure, which is required to compensate the variations in the distance between the flying arrow and the camera. We set the reference of length scale along the line connecting the launching nozzle and the target center. If the arrow flies closer to (or further from) the camera, its velocity is estimated faster (or slower) than its true value. This leads to erroneous estimates of the velocity, as illustrated in Figure 7. This figure shows the results of 36 shots by the expert female archer, who was asked to make horizontal scatter intentionally. The horizontal axis denotes the horizontal deviation h (mm) of the arrow at the target from the target center. The plus (or minus) sign means that the arrow deviates to right (or left). The vertical axis denotes the velocity U_2 obtained from the video image of Camera 2. We can see a clear correlation with a positive inclination between them. We determine the most probable inclination by a suitable data-fitting method. Then, we make a correction to each of data by drawing a line with the most probable inclination through each data point and computing the U_2-axis cross point. Similarly, we correct the velocity U_1 at Camera 1 and the corrected values are used in the following data-analysis. This empirical correction works quite well even if the arrow deviates from the target center considerably (more than ± 200 mm).

We estimate the drag exerted on the arrow by two methods, whose details are explained in Appendix. The first method uses the ratio between the horizontal velocity components at the two cameras. The second utilizes, in addition, the change of the attitude of the arrow, i.e., the angles of the arrow

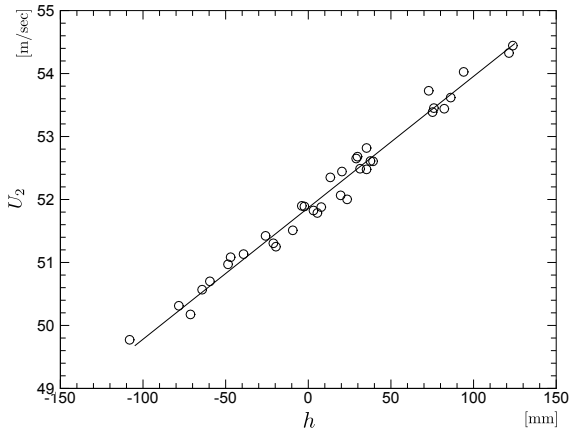

Fig. 7 Correlation between the horizontal velocity component U_2 at Camera 2 and the horizontal deviation h from the target center. The solid line represents the least squares line

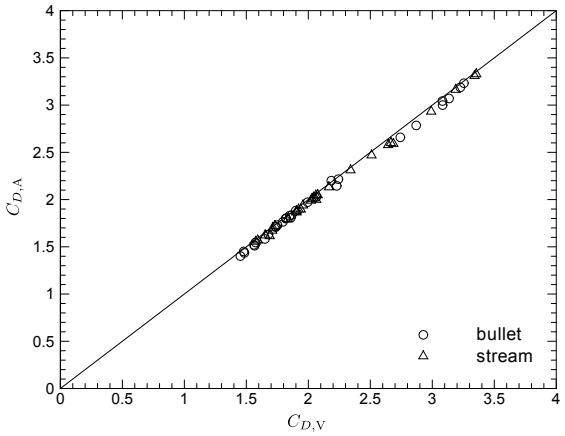

Fig. 8 Correlation between C_D values obtained by the two data analyses, i.e., using the velocity ratio ($C_{D,\mathrm{V}}$) and the arrow attitude ($C_{D,\mathrm{A}}$). The line $C_{D,\mathrm{V}} = C_{D,\mathrm{A}}$ is also shown

shaft measured from the horizontal plane. Both estimates coincide each other, if only the gravity and the drag act on the arrow (i.e., no lift). We show, in Fig. 8, the correlation between two values of the drag coefficient C_D of the arrow with the bullet (circles) and streamlined (triangles) points, in which the Re number is 1.3×10^4. We can see that two values of C_D deduced by the two data-analysis procedures coincide fairly well.

In the following results, we adapt only the data for which two values of C_D are identical within 3 %. We plot the mean of two values as a function of Re, in Figure 9. The horizontal axis is the Re number and the vertical axis denotes the drag coefficient C_D. The flight experiments cover the range

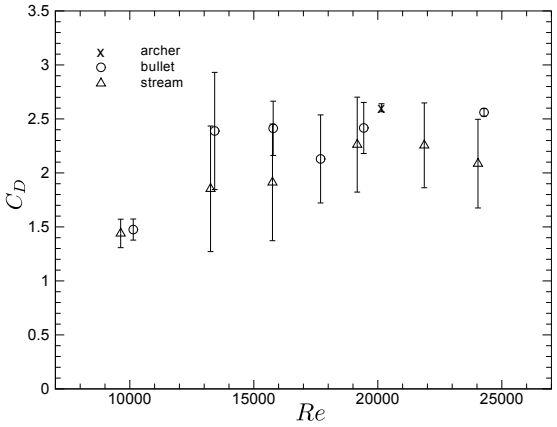

Fig. 9 C_D as a function of Re: Flight experiments

$0.9 \times 10^4 < Re < 2.4 \times 10^4$. The open circles show the data for the bullet point and the open triangles are for the streamlined point. The error bars denote the standard deviations.

We notice that the C_D values at low Re numbers (around 1.0×10^4) coincide with those from the wind tunnel tests, confirming the consistency of our two measurements. They are about 1.45 with the relative errors less than 8 %, and we suspect that the boundary layer on the arrow shaft remains laminar even in the free flight.

A drastic change is observed at higher Re numbers $Re > 1.3 \times 10^4$, showing a gradual increase in the mean C_D with an abrupt expansion of the relative error. However, the large relative errors do not mean the deterioration of the accuracy of our measurements. Instead, they indicate the occurrence of an important physical phenomenon, i.e., the transition from the laminar to the turbulent boundary layer. We will discuss this in detail in the next paragraph. As Re increases further (around $Re = 2.4 \times 10^4$), the drag coefficient C_D of the arrow with the bullet point increases to about 2.6 with a relative error less than 1.5 %. This suggests that the transition is completed by $Re = 2.4 \times 10^4$ (in the case of the bullet point). If the streamlined point is attached to the arrow nose, the transition seems not to be completed even at $Re = 2.4 \times 10^4$. The thick cross in Figure 9, shows the drag coefficient of the arrow launched by the expert female archer of the national team. The drag coefficient C_D is about 2.6 at $Re = 2.0 \times 10^4$ (58 m/sec), representing that the boundary layer is turbulent. The relative error is very small, being less than 3 %. This value may represent the accuracy of our measurements, which increases with Re. It is noted that the repeatability of her shots is remarkably high.

We show in Figs. 10 (bullet point) and 11 (streamlined point) the distributions of C_D values obtained in the flight experiments for several Re numbers. We see in Figure 10 that the distributions both at the lowest $Re = 1.0 \times 10^4$ and at the highest $Re = 2.4 \times 10^4$ are of Gaussian type. The mean values of C_D

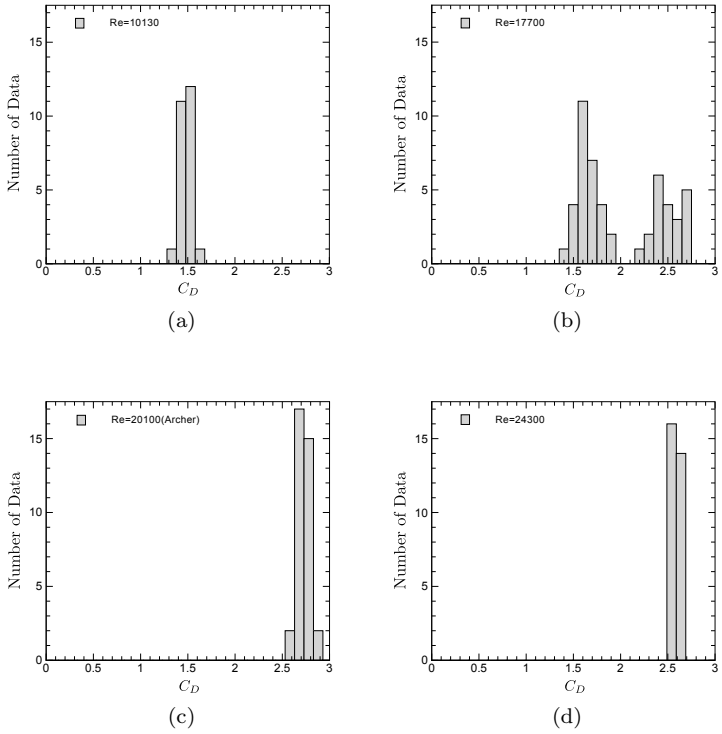

Fig. 10 Distributions of C_D at (a) $Re = 1.0 \times 10^4$, (b) 1.8×10^4, (c) 2.0×10^4, and (d) 2.4×10^4: Bullet point

are 1.45 and 2.6 with the relative errors 8 % and 1.5 %, respectively. The lower value of C_D corresponds to the laminar boundary layer and the larger value to the turbulent boundary layer. It is clear that the boundary layer transition on the arrow shaft with the bullet point occurs at a certain Re number between $Re = 1.0 \times 10^4$ and $Re = 2.4 \times 10^4$. However, it is not easy to determine the critical Reynolds number Re_c, because the distributions of C_D in this Re range show rather curious behavior. It is usual and not surprising that, in the transition region, the standard deviations become large, but we also observe two heaps in the C_D distribution at $Re = 1.8 \times 10^4$. At first, we thought the number of data might be too small, and increased them to 60 shots. The two heaps have never merged but remained, as if there are two types of shot, i.e., the laminar and turbulent shots. Similar two heaps are observed in a wider Re range ($1.3 \times 10^4 < Re < 2.4 \times 10^4$) for the arrow with the streamlined point (Figure 11). The laminar shots are found even at the highest Re considered, although the weight of the turbulent shot becomes larger as Re increases.

In order to have a deeper insight, we combine the results of the wind tunnel tests with those of the flight experiments in Fig. 12. Here, we replot the latter results by separating the laminar and turbulent shots, whenever the

C_D distribution has two heaps for a given Re. In other words, we make two groups of shots, i.e., one group with higher C_D and the other with lower C_D, and calculate average C_D for each group. There is a certain arbitrariness in the way of choosing separation point. We adopt the following procedure, hoping that the resulting C_D values are not far from the true values: (i) if two heaps are completely separated [c.f., Fig. 10(b)], choose any point between the two heaps; (ii) if a separation point is not determined by (i) (e.g., the heaps are overlapped), we simply choose the separation point as the mean of the entire distribution.

An excellent consistency is obtained for Re less than $Re = 1.1 \times 10^4$, where the boundary layer is laminar and C_D is about 1.5. We notice inconsistency in the Re range between 1.2×10^4 and 1.5×10^4. The boundary layer in the wind tunnel tests remains laminar but the turbulent (in addition to the laminar) shots are realized in the flight experiments. The drag coefficient C_D of the laminar shot is about 1.7 and that of the turbulent shot is about 2.9 irrespective of the point shape. The reason why this discrepancy occurs will be discussed in the next section. As Re increases, the laminar shots become rarer and rarer, and only turbulent shots are found for the arrow with the bullet point, when Re exceeds about 1.9×10^4. In contrast, both shots are found even at the highest Re number (2.4×10^4), if the streamlined point is attached to the arrow nose. This difference is surely linked with a profound nature of the boundary layer transition on the arrow shaft, which is left as a challenging future problem for researchers of fluid dynamics.

Before leaving this section, it is interesting to note that the distribution of C_D of the arrow launched by the archer has a Gaussian form (single heap) of the mean 2.65 and the relative error 3 % (Figs. 9 and 12). Although the Re number of her shots (about 2.0×10^4) is not much larger than 1.8×10^4, at which the number of laminar shots is larger than that of turbulent shots in our flight experiment, all her shots are turbulent shots (i.e., higher C_D). We suspect that the oscillation along the arrow shaft plays a key role in making the boundary layer turbulent.

4 Additional results from the wind tunnel tests and discussions

In this section. we consider the reason why the distributions of drag coefficient in the flight experiments have two heaps corresponding to the laminar and turbulent boundary layers. The major difference between the wind tunnel experiments and the flight experiments lies in the attitude of the arrow. In the MSBS wind tunnel tests, the attitude of the arrow is perfectly controlled to align with the flow and its angle of attack is kept to be strictly zero. The attitude of a flying arrow is also controlled by the attached vanes. The center of gravity lies well in front of the center of pressure and a stable flight is realized in general. However, the control of attitude is less perfect than in the MSBS wind tunnel. The flow is not strictly along the arrow shaft and therefore the

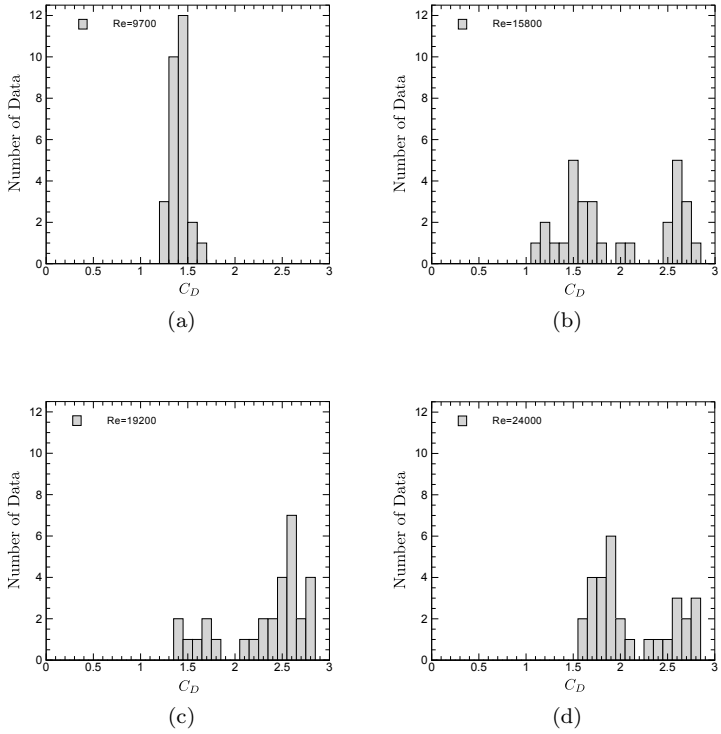

Fig. 11 Distributions of C_D at (a) $Re = 1.0 \times 10^4$, (b) 1.6×10^4, (c) 1.9×10^4, and (d) 2.4×10^4: Streamlined point

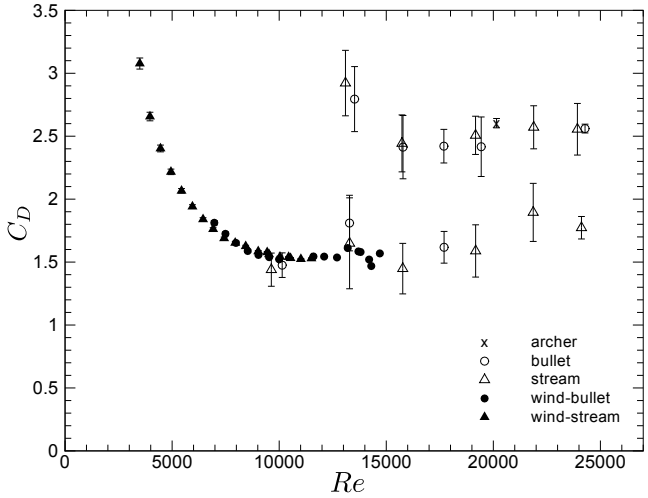

Fig. 12 C_D as a function of Re: Comparison between the results from MSBS wind tunnel tests and flight experiments

angle of attack is not zero, although it seems to be very small (less than 1 degree) from the video images.

The linear stability of the boundary layer on a cylinder surface was investigated by Tutty *et al.* [12] and Herrada et al. [5]. It is a difficult theoretical problem because the boundary layer develops along the cylinder. Tutty *et al.* [12] introduced a parallel flow approximation for a non-rotating cylinder and Herrada et al. [5] took the non-parallel flow effects into their analysis for a rotating cylinder surface. The most striking founding of Tutty *et al.* is that the critical Re number about 2.1×10^3 for the asymmetric bending mode ($m = 1$) is much smaller than the critical Re number about 2.4×10^4 for the axisymmetric mode ($m = 0$) mode. When the control of the arrow attitude is insufficient, the angle of attack becomes non-zero and bending mode ($m = 1$) disturbances are introduced to the boundary layer. We suspect that this explains why turbulent shots are observed in the flight experiments even at low Re number where the boundary layer remains laminar in the wind tunnel tests.

In order to check this possibility, we performed additional wind tunnel experiments. We can control the attitude of the arrow at will in the MSBS wind tunnel tests, and we investigate the dependence of C_D on the angle of attack θ in the range $|\theta| < 3$ deg. The results are shown in Fig. 13, in which the horizontal axis denotes the angle of attack θ and the vertical axis is measured C_D. The closed circles show the results for the bullet point at $Re = 1.0 \times 10^4$, whereas the open triangles are for the streamlined point at $Re = 1.0 \times 10^4$. When the angle of attack $|\theta|$ is smaller than about 0.6 deg, C_D is about 1.5 irrespective of the point shape and the boundary layer remains laminar. The drag coefficient C_D increases abruptly as $|\theta|$ exceeds about 1 deg, indicating that the laminar to turbulent transition of the boundary layer takes place even at $Re = 10^4$. Thus, the control of the attitude has a crucial influence on the nature of the boundary layer and thus on the drag coefficient. Although the attitude of the arrow in free flight is controlled by vanes and the angle of attack seems to be less than about 1 deg from the video images, the control is not enough to keep the boundary layer laminar at still higher Re numbers (say $Re > 1.3 \times 10^4$). The difference of the attitude of arrow explains the discrepancy between the results of the wind tunnel tests and those from the flight experiments.

When the angle of attack is non-zero, the lift F_L and the pitching moment M are exerted on the arrow besides the drag F_D. We can measure the lift and pitching moment coefficients in our wind tunnel tests. The lift coefficient C_L and the pitching moment coefficient C_M at $Re = 1.1 \times 10^4$ are plotted against the angle of attack θ in Fig. 14. The closed circles show C_L for the bullet point and the open triangles are for the streamlined point. The lift coefficient C_L is independent of the point shape, and the result for the streamlined point is shown. We notice that C_L is proportional to θ with a positive inclination about 0.69 deg^{-1}, indicating that the lift cannot be neglected even if the angle of attack is very small. Nevertheless our two data-analysis methods in the flight experiments, which assume no lift, provide the same values of C_D.

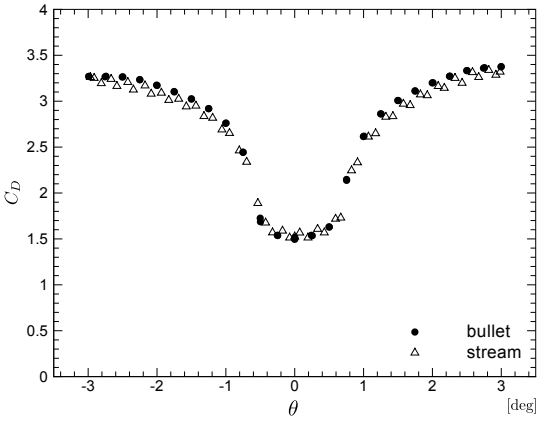

Fig. 13 C_D as a function of the angle of attack θ at $Re = 1.0 \times 10^4$

This is because the direction of the lift force changes, due presumably to the procession of the arrow, and the averaged lift becomes negligibly small.

This stabilization is assured by the negative inclination of the pitching moment coefficient C_M at $Re = 1.1 \times 10^4$. The closed squares show the results for the bullet point and the open diamonds are for the streamlined point. The pitching moment coefficient C_M is also irrelevant of the point shape, as in the case of C_L. It is proportional to the angle of attack θ with a negative inclination about -0.31 deg^{-1}, showing that the arrow is a stable projectile. We can estimate the position of the lift center from these results. It is located at about 30 cm rearward from the center of mass, i.e., at about 3 cm in front of the fletched vanes. Then, the lift and the pitching moment are mainly provided by the aerodynamic force acting on the vanes, confirming that the vanes play a key role in stabilizing the arrow flight.

As we have seen in the previous section, the boundary layer of the arrow launched by the archer is always turbulent, whose reason can be explained as follows. The oscillation along the arrow excites asymmetric disturbances at the point, which are advected into the boundary layer and induce the boundary layer transition. The arrow-oscillation is not only important in letting the vanes pass the bow handle (the so called archer's paradox) but also in making the boundary layer turbulent. Without this oscillation, the boundary layer might remain laminar occasionally, even in the Re range of arrows shot by archers, just as in the case of arrows launched by the blowing machine.

5 Conclusions

We have performed two support-interference-free measurements of aerodynamic forces exerted on an archery arrow (A/C/E; Easton). Two types of point, bullet and streamlined, are attached to the arrow nose, in order to clarify their influence on C_D. The MSBS wind tunnel tests show that the

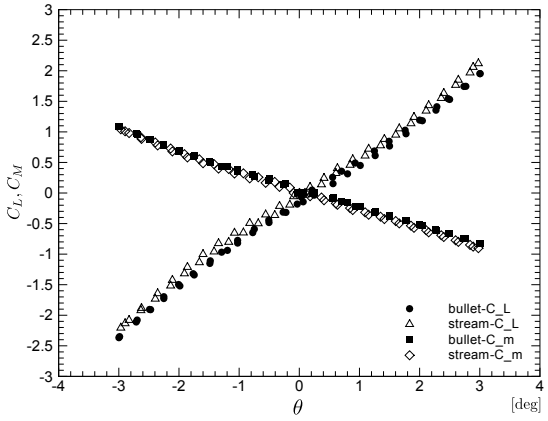

Fig. 14 C_L as a function of the angle of attack θ at $Re = 1.1 \times 10^4$

boundary layer of the arrow remains laminar in the measured Re number range ($4.0 \times 10^3 < Re < 1.5 \times 10^4$), and the drag coefficient is about 1.5 for $Re > 1.0 \times 10^4$, irrespective of the point shape. In the flight experiments, for which we developed a new arrow-shooting system using compressed air as a power source, we investigate Re number dependence of C_D in the range $9.0 \times 10^3 < Re < 2.4 \times 10^4$. The flight experiments support the the results from the wind tunnel tests in the range $Re < 1.2 \times 10^4$, for both points. When the bullet point is attached, the boundary layer becomes turbulent for $Re > 1.3 \times 10^4$ and the drag coefficient increases to about 2.6. Rather exceptionally, two values of C_D are found at $Re = 1.8 \times 10^4$. When the streamlined point is attached to the arrow nose, two values are found for $Re = 1.3 \times 10^4$ and the lower value is about 1.6 (laminar boundary layer) and the larger value is about 2.6 (turbulent boundary layer). The drag coefficient of the arrow launched by an expert archer is about 2.65 at $Re = 2.0 \times 10^4$ (58 m/sec). The reason why two values are observed in the flight experiments can be attributed to the insufficient control of the attitude of flying arrows. We show by MSBS wind tunnel tests that a very small angle of attack θ can induce the boundary layer transition even at $Re = 1.0 \times 10^4$. Similarly, the oscillation of the arrow from a bow makes the boundary layer turbulent.

We conclude this paper by estimating the ratio of mass to drag of the arrow (A/C/E) at a typical launching velocity 60 m/sec, whose value indicates the efficiency of the arrow as a projectile. This ratio is about 0.50 for the case of laminar boundary layer and increases to about 0.86 if the boundary layer becomes turbulent. We notice that this difference is not negligibly small, yielding about 15 cm difference in height at the target 70 m away. The shooting accuracy will be deteriorated seriously, if the boundary layer becomes turbulent or remains laminar, stochastically. Even if the velocity is unchanged, the Reynolds number decreases with the temperature and the possibility of a laminar boundary layer increases. It may be a safer strategy in archery tour-

naments to make the boundary layer turbulent intentionally, by adding some kind of roughness to the arrow-point.

Acknowledgements We are grateful to Prof. Hideo Sawada for his valuable advice in performing the MSBS wind tunnel tests. We also thank Prof. Ken Ohta, Dr. Seiji Sugimoto, and Takahiro Miwa for their kind support throughout the flight experiments at Japan Institute of Sports Sciences (JISS). This work is supported by JISS's "Team Japan Multi-support Project" entrusted from Ministry of Education, Culture, Sports, Science and Technology.

6 Appendix

We explain in this Appendix the details of two data-analysis methods used in order to estimate the drag coefficient C_D [11]. The first one is based on the ratio of the horizontal velocity components at Camera 1 and Camera 2. The second one utilize the change of arrow attitude with the gravitational acceleration g. Both methods assume that the forces acting on the arrow are the gravity and the drag, i.e., no lift is exerted on the arrow.

6.1 Method 1: using the horizontal velocity components

Under the previous assumption, the equations of motion are written as,

$$\frac{du}{dt} = -\frac{1}{2}\hat{D}u\sqrt{u^2+w^2}, \tag{3}$$

$$\frac{dw}{dt} = -g - \frac{1}{2}\hat{D}w\sqrt{u^2+w^2}, \tag{4}$$

$$\frac{ds}{dt} = \sqrt{u^2+w^2}. \tag{5}$$

Here, u and w denote the horizontal and vertical velocity components, respectively. The horizontal and vertical coordinates are x and z, respectively, and s means the length along the trajectory. The velocity decay rate $\hat{D}$ (m^{-1}) is linked with the drag coefficient C_D as

$$C_D = \frac{4m\hat{D}}{\rho\pi D^2}. \tag{6}$$

Here, m denotes the mass of the arrow.

We can eliminate the time variable t from (3) and (5):

$$\frac{du}{ds} = -\frac{1}{2}\hat{D}u. \tag{7}$$

It is solved to give a simple relation:

$$u = u_1 \exp\left(-\frac{1}{2}\hat{D}s\right). \tag{8}$$

Here, u_1 is the horizontal velocity component at Camera 1. Then we have $\hat{D}$ in the following form by putting $u = u_2$ with u_2 being the horizontal velocity component at Camera 2:

$$\hat{D} = -\frac{2}{s}\ln(\frac{u_2}{u_1}). \tag{9}$$

Although this relation is exact, it is not easy to determine trajectory length s between Camera 1 and Camera 2, analytically. When the initial velocity is very large, s can be approximated fairly well by the horizontal distance x between the two cameras. However, this approximation becomes too crude for a lower initial velocity, since in this case the vertical velocity component w_1 at Camera 1 cannot be neglected. We then approximate the trajectory by a parabola assuming the drag force is weak compared with the gravity:

$$s = \frac{u_1^2}{2g}\left[\left(\frac{gx}{u_1^2} - \sinh\xi_1\right)\sqrt{1+\left(\frac{gx}{u_1^2} - \sinh\xi_1\right)^2}\right.$$
$$\left. + \ln\left(\frac{gx}{u_1^2} - \sinh\xi_1 + \sqrt{1+\left(\frac{gx}{u_1^2} - \sinh\xi_1\right)^2}\right) + \frac{1}{2}\sinh(2\xi_1) + \xi_1\right]. \tag{10}$$

Here, a new variable $\dfrac{w_1}{u_1} = \sinh\xi_1$ is introduced, which is linked to the initial angle of arrow trajectory to the horizontal x-direction. We will see below that a similar variable is conveniently used in the second method of data-analysis.

6.2 Method 2: using the arrow attitude

The vertical component of the equations of motion (4) can be solved by using the variable $\dfrac{w}{u} = \sinh\xi$ or putting

$$w = u\sinh\xi(\mathrm{s}) = u_1\exp(-\frac{1}{2}\hat{D}s)\sinh\xi(\mathrm{s}). \tag{11}$$

Here, we use the relation (8). After some algebra, we find that the variable $\xi(s)$ is governed by the following differential equation:

$$\frac{d\xi}{ds} = -\frac{g}{u_1^2}\frac{\exp(\hat{D}s)}{\cosh^2\xi}, \tag{12}$$

in which time t is eliminated using (5) again. This equation is easily integrated to yield the following relation:

$$[\sinh 2\xi + 2\xi]_{\xi_1}^{\xi_2} = -\frac{4g}{u_1^2}\frac{\exp(\hat{D}s)-1}{D}$$
$$= \frac{4g}{\hat{D}}(\frac{1}{u_1^2} - \frac{1}{u_2^2}). \tag{13}$$

Since we know $\xi_{1,2}$ and $u_{1,2}$ from the video images, $\hat{D}$ is calculated using $g = 9.80\,\mathrm{m/sec^2}$. Note that the second method does not require the distance between the two cameras, and that it is more convenient in outdoor measurements.

References

1. Carrere P (1990) Contribution de la balistique au perfectionnement des etudes technofonctionnelles des pointesde projectiles prehistoriques, Paleo, 2: 167–176
2. Denny M (2003) Bow and catapult internal dynamics, Eur. J. Phys., 24: 367–378
3. Denny M (2011) Their arrows will darken the sky, 234. The Johns Hopkins University Press, Baltimore
4. Foley V, Palmer G and Soedel W (1985) The crossbow, Scientific American, 252(1): 104–110
5. Herrada MA, Pino CDel and Fernandez-Feria R (2008), Stability of the boundary layer flow on a long thin rotating cylinder, Phys. Fluids, 20: 034105
6. Kelly HR (1955) A note on the laminar boundary layer on a cylinder in axial compressible flow, J. Aerosp. Sci., 21: 634
7. Mukaiyama K, Suzuki K, Miyazaki T and Sawada H (2011) Aerodynamic properties of an arrow: Influence of point shape on the boundary layer transition, Proc. 5th Asia-Pacific Congress on Sports Technology, 13: 265–270
8. Sawada H (2007), Experimental study of aerodynamic performance of arrows with JAXA's 60cm magnetic suspension and balance system, Theoretical and Applied Mechanics Japan, 56: 237–242
9. Sawada H and Suda S (2011) Study on aerodynamic force acting on a sphere with and without boundary layer trips around the critical Reynolds number with a magnetic suspension and balance system, Exp. Fluids, 50: 271–284
10. Seban R A and Bond R (1951) Skin-friction and heat-transfer characteristics of a laminar boundary layer on a cylinder in axial compressible flow, J. Aerosp. Sci., 18: 671–675
11. Suzuki K, Masui K, Mukaiyama K, Miyazaki T and Sawada H (2010) Aerodynamic properties of an arrow: Influence of point-shape on the boundary layer transition, Nagare (J. Japan Soc. of Fluid Mechanics: in Japanese), 29(4): 287–296
12. Tutty OR, Price WG and Parsons A (2002) Boundary layer flow on a long thin cylinder, Phys. Fluids, 14(2): 628–637
13. Zanevsky I (2006) Bow tuning in the vertical plane, Sports Engineering, 9: 77–86